

OFFICIAL ORGAN OF THE RADIATION RESEARCH SOCIETY

RADIATION RESEARCH

EDITOR-IN-CHIEF: DANIEL BILLEN

Volume 84, 1980



ACADEMIC PRESS

New York London Toronto Sydney San Francisco

BIBLIOTHEK
der Tierärztlichen Fakultät
Königsplatz 10
8000 München 22

Copyright © 1980 by Academic Press, Inc.

All rights reserved

No part of this publication may be reproduced or transmitted in any form or by any means, electronic or mechanical, including photocopy, recording, or any information storage and retrieval system, without permission in writing from the copyright owner.

The appearance of the code at the bottom of the first page of an article in this journal indicates the copyright owner's consent that copies of the article may be made for personal or internal use, or for the personal or internal use of specific clients. This consent is given on the condition, however, that the copier pay the stated per copy fee through the Copyright Clearance Center, Inc. (21 Congress Street, Salem, Massachusetts 01970), for copying beyond that permitted by Sections 107 or 108 of the U.S. Copyright Law. This consent does not extend to other kinds of copying, such as copying for general distribution, for advertising or promotional purposes, for creating new collective works, or for resale. Copy fees for pre-1980 articles are the same as those shown for current articles.

MADE IN THE UNITED STATES OF AMERICA



Editor-in-Chief: DANIEL BILLEN, University of Tennessee–Oak Ridge Graduate School of Biomedical Sciences, Biology Division, Oak Ridge National Laboratory, P.O. Box Y, Oak Ridge, Tennessee 37830

Managing Technical Editor: MARTHA EDINGTON, University of Tennessee–Oak Ridge Graduate School of Biomedical Sciences, Biology Division, Oak Ridge National Laboratory, P.O. Box Y, Oak Ridge, Tennessee 37830

ASSOCIATE EDITORS

- | | |
|---|--|
| H. I. ADLER, Oak Ridge National Laboratory | S. LIPSKY, University of Minnesota |
| J. W. BAUM, Brookhaven National Laboratory | S. OKADA, University of Tokyo, Japan |
| S. S. BOGGS, University of Pittsburgh | N. L. OLEINICK, Case Western Reserve University |
| J. M. BROWN, Stanford University | A. M. RAUTH, Ontario Cancer Institute, Toronto, Canada |
| S. S. DONALDSON, Stanford University | M. C. SAUER, JR., Argonne National Laboratory |
| J. D. EARLE, Mayo Clinic | S. P. STEARNER, Argonne National Laboratory |
| J. J. FISCHER, Yale University | R. C. THOMPSON, Battelle, Pacific Northwest Laboratories |
| E. W. GERNER, University of Arizona | J. E. TURNER, Oak Ridge National Laboratory |
| E. L. GILLETTE, Colorado State University | S. S. WALLACE, New York Medical College |
| R. H. HUEBNER, Argonne National Laboratory | |
| J. W. HUNT, Ontario Cancer Institute, Toronto, Canada | |

OFFICERS OF THE SOCIETY

President: ODDVAR F. NYGAARD, National Cancer Institute, National Institutes of Health, Bethesda, Maryland 20205

Vice President and President-Elect: MORTIMER M. ELKIND, Division of Biological and Medical Research, Argonne National Laboratory, Argonne, Illinois 60437

Secretary-Treasurer: ROBERT B. PAINTER, Laboratory of Radiobiology, University of California, San Francisco, California 94143

Secretary-Treasurer-Elect: EDWARD R. EPP, Department of Radiation Medicine, Massachusetts General Hospital, Boston, Massachusetts 02114

Editor-in-Chief: DANIEL BILLEN, University of Tennessee–Oak Ridge Graduate School of Biomedical Sciences, Biology Division, Oak Ridge National Laboratory, P.O. Box Y, Oak Ridge, Tennessee 37830

Executive Director: RICHARD J. BURK, JR., 4720 Montgomery Lane, Suite 506, Bethesda, Maryland 20014

ANNUAL MEETINGS

1981: May 31–June 4, Minneapolis, Minnesota

1982: April 18–22, Salt Lake City, Utah

Titus C. Evans, Editor-in-Chief Volumes 1–50
Oddvar F. Nygaard, Editor-in-Chief Volumes 51–79



Councilors Radiation Research Society 1980–1981

PHYSICS

M. Inokuti, Argonne National Laboratory

H. J. Burki, University of California, Berkeley

BIOLOGY

J. S. Rasey, University of Washington

A. M. Rauth, Ontario Cancer Institute, Toronto, Canada

MEDICINE

H. D. Suit, Massachusetts General Hospital

J. A. Belli, Harvard Medical School

CHEMISTRY

J. F. Ward, University of California, San Diego

M. Z. Hoffman, Boston University

AT-LARGE

L. A. Dethlefsen, University of Utah

R. M. Sutherland, University of Rochester

CONTENTS OF VOLUME 84

NUMBER 1, OCTOBER 1980

LUO ZHENG-MING. An Electron Transport Theory of Cavity Ionization	1
M. R. RAJU, T. S. JOHNSON, N. TOKITA, S. CARPENTER, AND J. H. JETT. Differences in Cell-Cycle Progression Delays after Exposure to ^{238}Pu α Particles Compared to X Rays	16
E. BEN-HUR, H. UTSUMI, AND M. M. ELKIND. Potentially Lethal and DNA Radiation Damage: Similarities in Inhibition of Repair by Medium Containing D_2O and by Hypertonic Buffer	25
ERIK BOYE. DNA Repair and Replication in Cells of <i>Escherichia coli</i> Made Permeable with Hypotonic Buffers	35
ANAS M. EL-NAGGAR, ISMAIL R. A. HANNA, ARJUN D. CHANANA, ARLAND L. CARSTEN, AND EUGENE P. CRONKITE. Bone Marrow Changes after Localized Acute and Fractionated X Irradiation	46
ULRICH BERTSCHE AND BERNARD LACHET. The Response of Diploid Yeast to Radiations at Different LET. II. Analysis of Survival Data with Various Models of Radiation Action	53
P. J. NIJWEIDE, E. H. BURGER, J. L. VAN DELFT, E. W. M. KAWILARANG-DE HAAS, A. M. WASSENAAR, AND J. H. MELLINK. Effects of γ Irradiation on Cartilage Matrix Calcification	65
F. ZAMPETTI-BOSSSELER, PH. DELHAISE, AND S. LIMBOSCH. Ultraviolet Survival and Sensitizing Effect of Caffeine in Mouse Hybrid Cells	77
J. H. HENDRY, J. M. EDMUNDSON, AND C. S. POTTEN. The Radiosensitivity of Hair Follicles in Mouse Dorsum and Tail	87
D. W. WHILLANS AND A. M. RAUTH. An Experimental and Analytical Study of Oxygen Depletion in Stirred Cell Suspensions	97
BASIL V. WORGUL AND GEORGE R. MERRIAM, JR. The Lens Epithelium and Radiation Cataracts. II. Interphase Death in the Meridional Rows?	115
GEOFFREY MCLENNAN, LARRY W. OBERLEY, AND ANNE P. AUTOR. The Role of Oxygen-Derived Free Radicals in Radiation-Induced Damage and Death of Nondividing Eucaryotic Cells	122
E. L. TRAVIS, J. D. DOWN, S. J. HOLMES, AND B. HOBSON. Radiation Pneumonitis and Fibrosis in Mouse Lung Assayed by Respiratory Frequency and Histology	133

CORRESPONDENCE

HIROMICHI MATSUDAIRA, AKIKO M. UENO, AND IKUKO FURUNO. Iodine Contrast Medium Sensitizes Cultured Mammalian Cells to X Rays but not to γ Rays	144
CRAIG W. JONES, RAY D. LLOYD, AND CHARLES W. MAYS. Salicylic Acid Failed to Increase the Efficacy of Ca-DTPA in the Decorporation of Plutonium and Americium	149
M. R. RAJU, E. BAIN, S. G. CARPENTER, J. JETT, R. A. WALTERS, J. HOWARD, AND P. POWERS-RISIUS. Effects of Argon Ions on Synchronized Chinese Hamster Cells	152
M. R. RAJU, E. BAIN, S. G. CARPENTER, J. HOWARD, AND J. T. LYMAN. Cell-Survival Measurements as a Function of Depth for a High-Energy Argon-Ion Beam	158
EINAR SAGSTUEN. Radiation Damage to Nucleosides and Nucleotides. III. A C_4 -Centered Radical in the Ribose Moiety of Uridine-5'-phosphate Single Crystals	164

ANNOUNCEMENTS	171
-------------------------	-----

NUMBER 2, NOVEMBER 1980

A. M. KELLERER, D. CHMELEVSKY, AND E. J. HALL. Nonparametric Representation of Dose-Effect Relations	173
D. COMBECHER. Measurement of W Values of Low-Energy Electrons in Several Gases	189
D. CHMELEVSKY, A. M. KELLERER, M. TERRISSOL, AND J. P. PATAU. Proximity Functions for Electrons up to 10 keV	219

D. R. WHITE, L. H. J. PEAPLE, AND T. J. CROSBY. Measured Attenuation Coefficients at Low Photon Energies (9.88–59.32 keV) for 44 Materials and Tissues	239
MOHAMMAD A. SAMI. Pulse Radiolysis of Solutions of Anthracene in Liquid Methylamine at 298 K	253
R. A. DELLA GUARDIA AND F. J. JOHNSTON. Radiation-Induced Reaction of Sulfur and Water	259
SHIGEKAZU NAKATSUGAWA AND TSUTOMU SUGAHARA. Inhibition of X-Ray-Induced Potentially Lethal Damage (PLD) Repair by Cordycepin (3'-Deoxyadenosine) and Enhancement of Its Action by 2'-Deoxycoformycin in Chinese Hamster <i>hai</i> Cells in the Stationary Phase <i>in Vitro</i>	265
R. M. HENKELMAN, G. K. Y. LAM, R. O. KORNELSEN, AND C. J. EAVES. Explanation of Dose-Rate and Split-Dose Effects on Mouse Foot Reactions Using the Same Time Factor	276
G. A. KING, J. O. ARCHAMBEAU, AND R. R. KLEVECZ. Survival and Phase Response following Ionizing Radiation and Hyperthermia in Synchronous V79 and EMT6 Cells	290
A. G. UNDERBRINK AND BARBARA WOCH. Evidence That the Oxygen Enhancement Ratio for Pink Somatic Mutations in <i>Tradescantia</i> Stamen Hairs May Approach Unity at Very Low X-Ray Doses	301
J. L. MAUDERLY, B. A. MUGGENBURG, F. F. HAHN, AND B. B. BOECKER. The Effects of Inhaled ¹⁴⁴ Ce on Cardiopulmonary Function and Histopathology of the Dog	307
F. W. BRUENGER, W. STEVENS, B. J. STOVER, G. N. TAYLOR, J. M. SMITH, D. S. BUSTER, AND D. R. ATHERTON. The Distribution and Pathological Effects of Pu in Juvenile Beagles	325
J. M. GEARHART, J. H. DIEL, AND R. O. MCCLELLAN. Intrahepatic Distribution of Plutonium in Beagles	343

CORRESPONDENCE

CARTER B. SCHROY, PAUL S. FURCINITTI, PAUL TODD, AND NANCY E. KUKULINSKY. Potentiation by Caffeine of Potentially Lethal Fast-Neutron Damage in Cultured Human Cells	353
--	-----

ANNOUNCEMENTS	359
-------------------------	-----

NUMBER 3, DECEMBER 1980

THE BEIR III CONTROVERSY

JACOB I. FABRIKANT. The BEIR III Controversy	361
EDWARD P. RADFORD. Human Health Effects of Low Doses of Ionizing Radiation: The BEIR III Controversy	369
HARALD H. ROSSI. Comments on the Somatic Effects Section of the BEIR III Report	395
A. I. KASSIS, S. J. ADELSTEIN, C. HAYDOCK, AND K. S. R. SASTRY. Radiotoxicity of ⁷⁵ Se and ³⁵ S: Theory and Application to a Cellular Model	407
JOHN C. HAYNES, SHIN-ICHI KURODA, KIYOSHI MATSUKI, AND ICHIRO MIYAGAWA. ESR and ENDOR Studies of X-Irradiated <i>N</i> -Acetyl-D,L-Alanine	426
ROBERT E. MILLS AND HARALD H. ROSSI. Mean Energy Deposition Distribution about Proton Tracks	434
M. DI PAOLA, V. CAFFARELLI, M. COPPOLA, F. PORRO, M. QUINTILIANI, J. BAARLI, M. BIANCHI, AND A. H. SULLIVAN. Biological Responses to Various Neutron Energies from 1 to 600 MeV. I. Testes Weight Loss in Mice	444
M. DI PAOLA, M. COPPOLA, J. BAARLI, M. BIANCHI, AND A. H. SULLIVAN. Biological Responses to Various Neutron Energies from 1 to 600 MeV. II. Lens Opacification in Mice	453
M. H. SCHNEIDERMAN AND K. G. HOFER. The Target for Radiation-Induced Division Delay	462
M. A. O'LOUGHLIN, D. W. WHILLANS, AND J. W. HUNT. A Fluorescence Approach to Testing the Diffusion of Oxygen into Mammalian Cells	477
Y. ASHANI, F. H. HENRY, AND G. N. CATRAVAS. Combined Effects of Anticholinesterase Drugs and Low-Level Microwave Radiation	496
RAYMOND L. WARTERS, JOSEPH L. ROTI ROTI, AND R. TERRY WINWARD. Nucleosome Structure in Chromatin from Heated Cells	504

YUKIKO MANO, HIROSHI MITANI, HISAMI ETOH, AND NOBUO EGAMI. Survival and Photoreactivity of Ultraviolet-Irradiated Cultured Fish Cells (CAF-MM1)	514
R. TIMOTHY MULCAHY, MICHAEL N. GOULD, AND KELLY H. CLIFTON. The Survival of Thyroid Cells: <i>In Vivo</i> Irradiation and <i>in Situ</i> Repair	523
C. ANNE WALLEN, SOLOMON M. MICHAELSON, AND KENNETH T. WHEELER. Evidence for an Unconventional Radiosensitivity of Rat 9L Subcutaneous Tumors	529
R. A. S. WHITE, P. WORKMAN, AND J. M. BROWN. The Pharmacokinetics and Tumor and Neural Tissue Penetrating Properties of SR-2508 and SR-2555 in the Dog—Hydrophilic Radiosensitizers Potentially Less Toxic than Misonidazole	542
BERNARD C. ZOOK, EILEEN W. BRADLEY, GEORGE W. CASARETT, AND CHARLES C. ROGERS. Pathologic Findings in Canine Brain Irradiated with Fractionated Fast Neutrons or Photons ..	562
CORRESPONDENCE	
J. M. SMITH, G. N. TAYLOR, AND W. S. S. JEE. A Technique of Neutron-Induced (Fission-Track) Autoradiography with Histological Detail	579
R. F. JOSTES, JR. AND R. B. PAINTER. Evidence for Repair of Premutational Damage from Split X-Ray Doses	586
BOOK REVIEWS	591
AUTHOR INDEX FOR VOLUME 84	594
CUMULATIVE SUBJECT INDEX FOR VOLUMES 81–84	596

Proximity Functions for Electrons up to 10 keV¹

D. CHMELEVSKY AND A. M. KELLERER

*Institut für Medizinische Strahlenkunde der Universität Würzburg, Versbacher Str. 5,
Würzburg D-8700, Germany*

AND

M. TERRISSOL AND J. P. PATAU

Centre de Physique Atomique, Université Paul Sabatier, Toulouse Cedex F-31077, France

CHMELEVSKY, D., KELLERER, A. M., TERRISSOL, M., AND PATAU, J. P. Proximity Functions for Electrons up to 10 keV. *Radiat. Res.* 84, 219-238 (1980).

Proximity functions for electrons up to 10 keV in water are computed from simulated particle tracks. Numerical results are given for the differential functions $t(x)$ and the integral functions $T(x)$. Basic characteristics of these functions and their connections to other microdosimetric quantities are considered. As an example of the applicability of the proximity functions, the quantity \bar{y}_D for spheres is derived from $t(x)$.

INTRODUCTION

The major part of microdosimetric data has been obtained in the past by experimental methods. Some computations have been performed but most have been somewhat simplified (1-6). Only recently methods have been developed to simulate numerically the full complexity of the tracks of charged ionizing particles. This has been achieved by Monte Carlo calculations based on theoretical and experimental cross sections (7-14). At present there are no experimental techniques for the determination of microdosimetric data for tissue volumes with linear dimensions smaller than about 0.3 μm ; for very small regions the computational method is therefore the only practicable approach.

A few years ago simulated proton tracks by Paretzke *et al.* (8, 9) were used to obtain microdosimetric data for heavy ions and for sites of 5 to 100 nm in diameter (15, 16). These studies led, apart from numerical data, to concepts and quantities (17-19) beyond those that had been previously established in microdosimetry. A particularly important concept, the proximity function of energy transfers, had been proposed earlier (20, 21) as a fundamental description of track structure. However, it was only in the context of the numerical calculations that the actual applicability of the proximity function and its close connection to conventional microdosimetric quantities such as ζ or \bar{y}_D became apparent [for the definition of microdosimetric quantities see (22)]. Moreover, it was realized that

¹ Work supported by Euratom Contracts 208-B10 D and 176 B10 F.

the function is relevant to a biophysical argumentation that deals with the interaction of pairs of radiation-induced sublesions (23, 24).

Accordingly, it is desirable to obtain proximity functions for various radiation qualities. Although the Monte Carlo programs for the simulation of charged particle tracks are well developed, a systematic effort has not yet been made to generate complete sets of proximity functions for the most important radiation qualities. As a step toward establishing the necessary data, we have therefore derived these functions for electrons up to 10 keV in water.

DEFINITION OF THE PROXIMITY FUNCTION

A convenient definition of the proximity function (also termed distance distribution or, for brevity, t function) is obtained in terms of the integral distribution.

Definition. The integral function $T(x)$ is the expected energy imparted due to the same particle track within the distance x around an energy transfer chosen at random. The energy transfer chosen as reference is included in $T(x)$.

The term *energy transfer* designates energy locally transferred from the ionizing radiation field to the material. If an ionizing particle undergoes an interaction at a point (the *transfer point*) the energy transfer ϵ is equal to the kinetic energy of the incoming particle minus the kinetic energy of any emerging ionizing particle(s). A more rigorous definition has to account also for possible changes of rest mass (17, 25), but this is of no concern in the present context.

The term *particle track* designates the set of all energy transfers due to the same primary particle and its secondaries.

In the random choice of the energy transfer the magnitude of the energy transfer is used as a weight factor; i.e., each energy transfer ϵ has a probability of being selected that is proportional to ϵ [for a detailed discussion of the sampling procedure see (15, 18)].

Although one could refer to a more general situation, the present definition applies to a uniform medium of density ρ . $T(x)$ depends on the composition of the irradiated medium (usually tissue or water) and on the type of radiation.

The definition of $T(x)$ can also be given in terms of a summation over all energy transfers of interest, i.e., without reference to random sampling:

$$T(x) = \sum_{i,k} \epsilon_i \epsilon_k / \sum_i \epsilon_i, \quad x_{ik} < x, \quad (1)$$

where the summation in the denominator extends over all energy transfers ϵ_i and the double summation in the numerator runs over all energy transfers ϵ_i and over those energy transfers ϵ_k (including $i = k$) that are on the same track and are separated from ϵ_i by a distance x_{ik} not larger than x .

A more general proximity function $T_D(x)$ includes not only energy transfers on the same particle track but also the contribution from other statistically independent particle tracks, and accordingly depends on absorbed dose. However, it has been shown (19) that $T_D(x)$ differs from $T(x)$ only by a trivial term

$$T_D(x) = T(x) + (4/3)\pi x^3 \rho D, \quad (2)$$

$T(x)$ represents the *intratrack* contribution, while the second term represents

the *intertrack* contribution. Since the *intertrack* contribution is of such simple form and independent of radiation quality, it is sufficient to consider $T(x)$.

The differential *t* function is defined as the derivative of the integral *t* function

$$t(x) = \frac{dT(x)}{dx} . \tag{3}$$

In the following, *t* functions $t_E(x)$ are given for electrons of specified initial energy E . One can readily show that for a mixed field of electrons one obtains

$$t(x) = \int_0^\infty t_E(x)En(E)dE \Big/ \int_0^\infty En(E)dE, \tag{4}$$

$n(E)$ is the frequency distributions of the initial energies of the electrons. The formula for $T(x)$ is analogous.

An important property of $t(x)$ is that it is proportional to the probability density of distances between pairs of energy transfers randomly chosen in the irradiated medium. From Eq. (4) it follows that the normalization factor is equal to the dose-weighted average $\langle E \rangle$ of the energy per charged particle track:

$$\begin{aligned} \int_0^\infty t(x)dx &= \int_0^\infty \int_0^\infty t_E(x)En(E)dEdx \Big/ \int_0^\infty En(E)dE \\ &= \int_0^\infty E^2n(E)dE \Big/ \int_0^\infty En(E)dE = \langle E \rangle. \end{aligned} \tag{5}$$

The fact that $t(x)$ is not normalized to unity is merely a matter of convenience that facilitates the consideration of extended regions and particles of large energy.

RELATION TO LINEAR ENERGY TRANSFER AND TO CONVENTIONAL MICRODOSIMETRIC QUANTITIES

The functions $T(x)$ or $t(x)$ offer a mathematical representation of the micro-distribution of energy imparted; as such they have direct applicability in radiation biophysics (23, 24). However, the functions are also related to the dose average linear energy transfer \bar{L}_D , and they are linked to some of the established micro-dosimetric quantities. The relations that have been considered earlier (22, 23) will be listed without derivation.

In the simplest LET approximation, where linear tracks with constant rate of energy transfer are considered and where no account is taken of their finite range, one obtains, as can be shown from Eq. (4),

$$t(x) = 2 \bar{L}_D. \tag{6}$$

The relation to microdosimetric quantities results from the fact that $t(x)$ permits the calculation of the distribution $v(x)$ of distances of transfers *within* a specified region from the function $t(x)$ that refers to an extended medium,

$$v(x) = s(x)t(x)/4\pi\rho x^2, \tag{7}$$

$s(x)$ is a function that characterizes the region of interest and that is analogous to the function $t(x)$. It is the distribution of distances between points of the region

multiplied by the mass of the region. One can also say that $s(x)dx$ is the expected mass of the region within a spherical shell of radius x and thickness dx that is centered at a point randomly chosen in the region. As with $t(x)$, the function $v(x)$ is not normalized to unity. Instead one finds that the normalization factor is equal to the microdosimetric quantity $\bar{\epsilon}_D$, i.e., the dose average energy imparted per event in the region (19, 25):

$$\bar{\epsilon}_D = \int_0^{\infty} v(x)dx = \int_0^{\infty} \frac{s(x)t(x)}{4\pi\rho x^2} dx. \quad (8)$$

The relation is important because it shows that one single function, characterizing the radiation field, permits the computation of $\bar{\epsilon}_D$ for regions of any shape and size, as well as the computation of the closely related quantities ζ or \bar{y}_D .

For a sphere of diameter d one has

$$s(x) = 4\pi\rho x^2 \left(1 - \frac{3}{2} \frac{x}{d} + \frac{x^3}{2d^3} \right) \quad \text{for } x \leq d, \quad (9)$$

and therefore

$$\bar{\epsilon}_D = \int_0^d \left(1 - \frac{3}{2} \frac{x}{d} + \frac{x^3}{2d^3} \right) t(x) dx. \quad (10)$$

Equations (7) and (8) make it unnecessary to repeat explicit calculations, or Monte Carlo simulations, for each geometry that may be considered and for each radiation of interest. Instead it is sufficient to compute the functions $t(x)$ for the different radiations and the functions $s(x)$ for the different geometries. The distribution $v(x)$ or the quantity $\bar{\epsilon}_D$ is then readily obtained for all possible combinations.

COMPUTATION OF THE DISTANCE DISTRIBUTIONS

The computation of the distance distributions $t(x)$ from simulated charged particle tracks is straightforward. The simulated particle tracks are given in terms of the Cartesian coordinates of the transfer points and the associated energy transfers. In the computation all energy transfers of all utilized tracks are considered, and for each of these the squares of the distances to other transfers from the same track are determined. All resulting values are stored in an array that refers to a distance grid with equal logarithmic steps. The scale is chosen so that successive grid points belong to a distance ratio $2^{1/32} = 1.022$. To cover the distance range from 0.1 nm to 100 μm , one then needs 638 points on the array.

Substantial computing times are involved. For a track of a 10-keV electron one has approximately 1000 energy transfers. Evaluation of one track therefore requires approximately 500,000 computations of distances. Since 100 tracks were evaluated, about 5×10^7 distances had to be computed and stored. It is therefore essential to avoid repeated computations of logarithms of the squared distances for assigning the location in the storage array. Accordingly the logarithmic storage address for each square of distance is obtained by a simplified operation in machine code that takes the place of the computation of a logarithm but requires only the time of roughly one addition. This decreases the total computing time for the program by more than a factor of 4 (on a TR 440) and reduces it to a fraction of an hour.

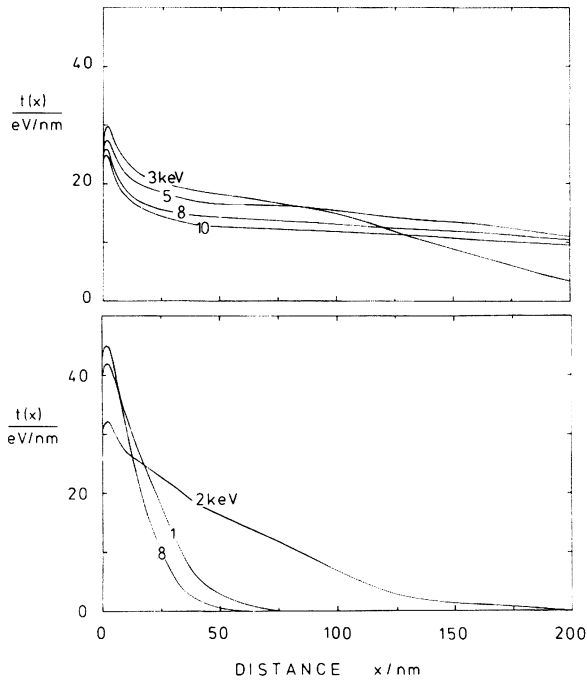


FIG. 1. Proximity functions for electrons of specified energy in water.

It was therefore not necessary to employ methods to reduce the number of distances to be computed. For higher electron energies such methods would be required.

The present computations are based on 100 tracks of electrons, with initial energy 10 keV in water, that were produced by the program of Terrissol and Patau. Some details of the program are described in Appendix A.

The *t* functions for initial energies 10, 8, 5, 3, 2, 1, 0.8, 0.5, 0.3, 0.2, and 0.1 keV were obtained simultaneously from the same tracks using separate storage arrays.

NUMERICAL RESULTS

Figures 1–5 represent the essential numerical results. Differential distributions *t*(*x*) for various energies are given in Fig. 1. The figure extends up to distances of 200 nm. This scale permits a convenient comparison of the characteristic shapes of the functions and their dependence on electron energy. However, at energies exceeding 2 keV the tails of the functions are not included. For this reason a separate plot is given in Fig. 2 of the proximity functions for energy exceeding 2 keV; this scale extends to the full range of the functions. On the other hand, even in Fig. 1 the scale is not fine enough to permit a clear representation of the proximity functions for energies below 0.8 keV. Figure 3 therefore gives a large-scale representation of the initial part of the proximity functions; in actual biophysical applications the curve shapes at small distances are of particular interest.

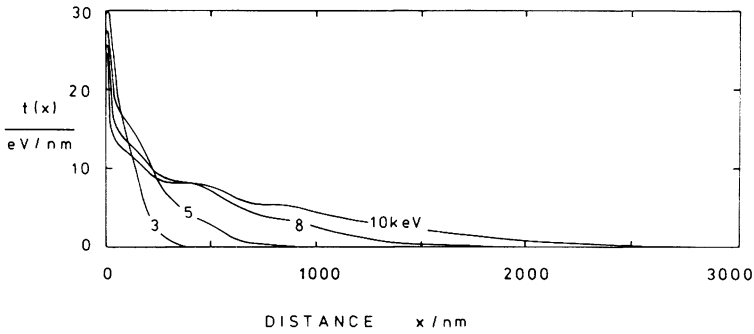


FIG. 2. Proximity functions for electrons of 3 to 10 keV in water. The functions are given on a scale that includes the tails of the distributions. The wave-like irregularities on the functions for 8- and 10-keV electrons may reflect statistical uncertainties due to the finite number of electron tracks.

The sum distributions $T(x)$ are also given in two different scales in Figs. 4 and 5. In these figures the broken curves are inserted for further illustration. They represent the contribution to the full distance distribution $T_D(x)$ [see Eq. (2)] of independent ionizing particles. This helps to visualize the relative magnitudes of the intratrack term (solid curves) and the intertrack term (broken curves) at the doses that are indicated. As stated earlier, the intertrack term is independent of radiation quality. The main point is that at small distances and at the doses of practical interest in radiobiology most of the neighboring energy transfers in the vicinity of a transfer belong to the same particle track. A somewhat different plot of the functions $T(x)$ that also contains the standard errors is given in Fig. 15 in Appendix A.

It must be noted that the differential distributions $t(x)$ contain δ -function terms at $x = 0$. These terms represent the energy transfers on the reference transfer points themselves. They are not shown in the plot of $t(x)$; however, they are the reason that the sum distributions start with finite values $T(0)$ at zero distance. These values are equal to the dose averages of the individual transfers

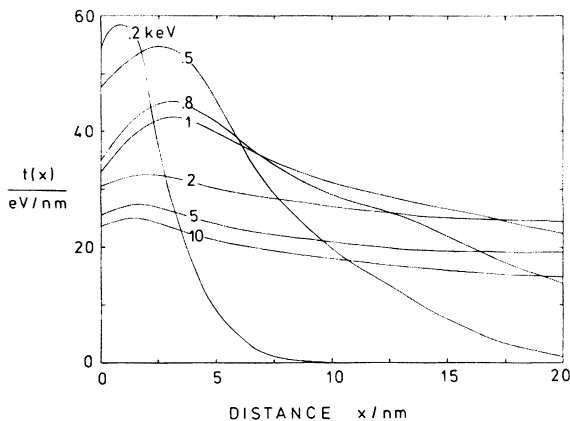


FIG. 3. Proximity functions for electrons in water on an extended scale that contains only the initial part of the functions.

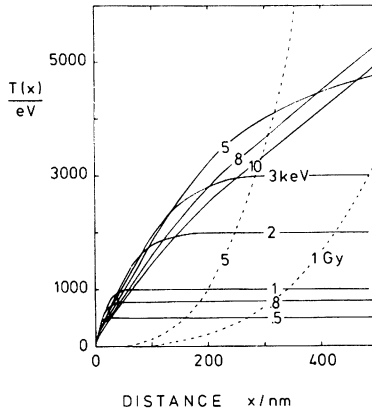


FIG. 4. Integral proximity functions for electrons of specified energy in water. The broken lines represent the intertrack contribution at doses of 1 and 5 Gy (see text).

$$T(0) = \sum_i \epsilon_i^2 / \sum_i \epsilon_i, \tag{11}$$

where the summation extends over all transfers. The resulting values range from $T(0) = 28$ eV for the electrons of 10 keV to $T(0) = 30$ eV for electrons of 0.5 keV.

At small distances the proximity functions have pronounced peaks, reflecting the very localized clustering of energy transfers in the charged particle tracks. The precise shape of the peaks may be affected by uncertainties in the collision cross sections at low energies. However, the exact dependence on x is of limited importance. Any degree of energy conduction or diffusion will remove some of the fine structure in the spatial correlation of energy transfers; this will have the general effect of reducing the magnitude of the energy concentrations over short distances.

Figures 6 and 7 demonstrate this effect of diffusion by an example. In these plots modified proximity functions that result if the patterns of energy transfers are subjected to diffusion with a characteristic distance $\Delta = 5$ nm are given. The char-

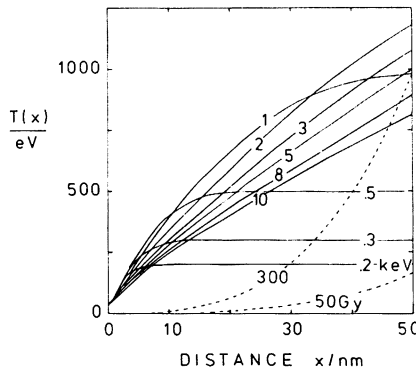


FIG. 5. Integral proximity functions for electrons of specified energy in water on an extended scale that contains only the initial part of the functions. The broken lines represent the intertrack contribution at doses of 50 and 300 Gy (see text).

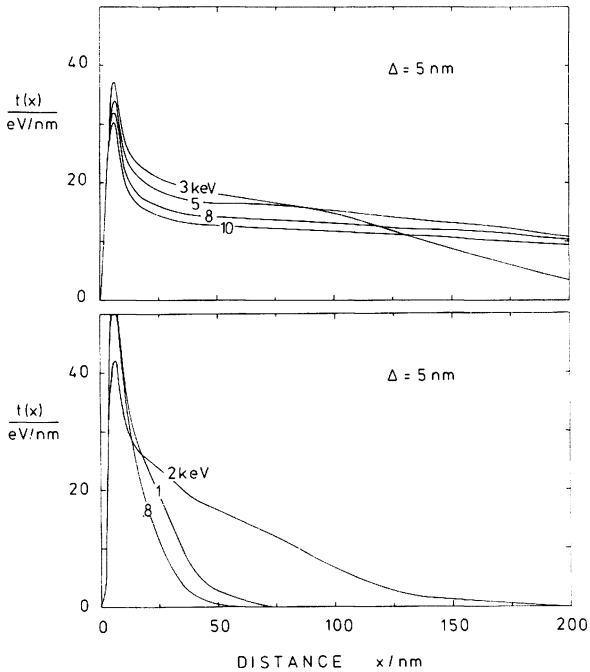


FIG. 6. Proximity functions for electrons in water that result if the inchoate pattern of energy transfers has diffused. The parameter $\Delta = 5$ nm characterizes the extent of the diffusion. It is equal to the mean separation that results for two points initially coinciding.

acteristic distance Δ is defined as the mean separation that results if two points, initially coinciding, are subjected to diffusion. The formulas that permit the derivation of the transformed distributions are listed in Appendix B.

The proximity functions can be used to derive the microdosimetric quantities

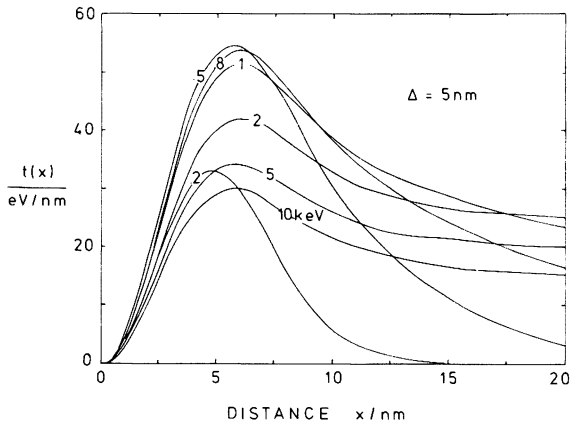


FIG. 7. Initial parts of the proximity functions for electrons in water that result if the inchoate pattern of energy transfers has diffused. The parameter $\Delta = 5$ nm characterizes the extent of the diffusion. It is equal to the mean separation that results for two points initially coinciding.

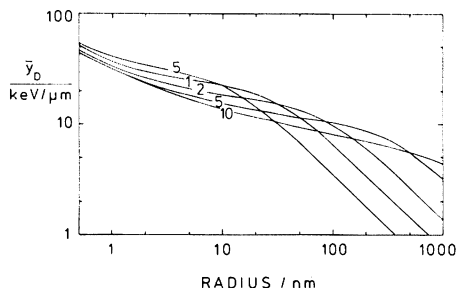


FIG. 8. The microdosimetric quantity \bar{y}_D for spheres calculated from the proximity functions (see Eq. (10)). The quantity \bar{y}_D is equal to $3\bar{\epsilon}_D/2d$, where d is the diameter of the sphere. The parameters on the curves give the electron energies in keV.

$\bar{\epsilon}_D$, ζ , or \bar{y}_D for various geometries. It is not the purpose of this article to treat this in detail, but a comprehensive plot of \bar{y}_D is given in Fig. 8 for the important case of a sphere.

As stated earlier, a systematic comparison of the data with those obtained from other simulated particle tracks is desirable but presently not feasible, since too few data are published. However, Table I summarizes the comparison with the limited data presently available. It shows good agreement between the present

TABLE I
Comparison to Earlier Results

<i>r</i> (nm)	$\bar{\epsilon}_D$				<i>T(x)</i>		
	Energy (keV)				<i>x</i> (nm)	Energy (keV)	
	0.5	1	5	10		0.5	5
2	105 (90)				2	100 (120)	
5	230 (190)	205 (170)	115 (120)		5	280 (260)	190 (160)
10	340 (300)				10	420 (410)	
25		625 (570)					
50		740 (770)	820 (770)	860 (620)	50		1010 (1000)
75		825 (840)					

Note. In the left-hand part of the table values $\bar{\epsilon}_D$ are listed that refer to cubical volumes of side length $2r$; they are derived from distributions of energy imparted or of numbers of ionizations published by Hamm *et al.* (13). Results for spherical volumes from the present calculations are in parentheses. In the right-hand part of the table values $T(x)$ are listed that are derived from distributions of numbers of ionizations published by Paretzke (26). Values from the present calculations are given in parentheses. In both sets of data the value $W = 30$ eV is used for conversion.

results and values $T(x)$ that can be estimated from results published by Paretzke (26). Data published by Hamm *et al.* (13) do not relate to the t function but to the frequency distributions of energy imparted to cubes. Values $\bar{\epsilon}_D$ derived from these distributions do not differ greatly from the values obtained in the present calculations for spherical volumes.

In the context of a treatment of diffusion in Appendix B a comparison is made with experimental data obtained from cloud chamber studies (27, 28).

FACTORS INVOLVED IN THE DISTANCE DISTRIBUTIONS

The distance distributions represent the spatial correlation of energy within the electron tracks. The main factors that are involved are total range and energy of the tracks, curvature of the tracks, and clustering of energy transfers along the tracks (δ rays).

For a better understanding of the properties of the t functions one must consider the influence of the δ rays. It has previously been shown (19) that the distance distribution can be separated into two terms:

$$t(x) = t_\delta(x) + t_a(x). \quad (12)$$

The first term $t_\delta(x)$ represents only those correlated energy transfers that result from the same collision of the primary electron; such correlated energy transfers resulting from the same primary collision will in the present context be designated by the term *delta*. This term will also be used for single transfers that result from a collision of the primary particle. The term *delta* is therefore not identical to the usual notion of a δ ray. The quantity $t_a(x)$ is the contribution from energy transfers not on the same *delta*.

The initial high values of the t functions represent correlated energy transfers within the same *delta*. Figure 9 illustrates this by separating t functions into the two components.

In biophysical considerations one uses, not infrequently, simplifications that depict the particle tracks by straight lines with continuous energy loss that varies along the track according to the dependence of linear energy transfer $L(s)$ on ranges. One can readily deduce the t functions that would result in this simplified model,

$$t(x) = \frac{2}{E} \int_0^{r_0} L(s-x)L(s)ds, \quad (13)$$

where r_0 is the continuous-slowning-down range (CSD range). The resulting curves are depicted in the panels of Fig. 10 by broken lines. All curves in Fig. 10 are plotted versus a normalized distance x/r_0 and are normalized to unity. This facilitates comparison of the curves for different energies. The simplified model leads to curves that are substantially different from the actual functions that are given as solid lines.

The straight lines are inserted to show that another model which is seemingly cruder lead, in fact, to a better agreement with the actual functions. This model approximates the electron tracks by straight line segments of length $2r_0/3$ with

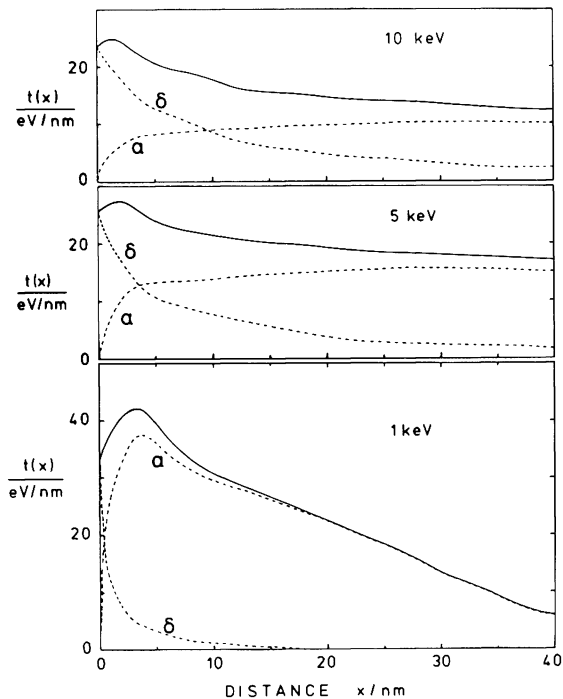


FIG. 9. Proximity functions for electrons of the specified energies in water, and their separation into the two components $t_\delta(x)$ and $t_\alpha(x)$ [see Eq. (12)].

constant rate of energy loss. The resulting t functions are given by the formula

$$t(x) = (3E_0/r_0)(1 - 3x/2r_0), \quad x \leq 2r_0/3. \tag{14}$$

The simplified model has frequently been invoked in dosimetric computations (29, 30), and it is supported by a consideration of the proximity functions.

COMPUTATIONS BASED ON THE NUMBER OF IONIZATIONS

A simplified approach pictures the charged particle tracks merely as a set of ionizations. This corresponds to the experimental approach in microdosimetry that utilizes ion collection and multiplication devices such as the Rossi counters (31). It is difficult to make theoretical statements on changes of the numerical values that result if microdosimetric quantities are derived on the basis of ionizations only rather than on the actual energy transfers.

For this reason the t functions have been computed in a simplified way that neglects all excitations and counts only the ionizations with the W values that result for the tracks of specified initial energies. The t functions obtained in this way differ very little from those based on the full data. This is illustrated in Fig. 11 where the results obtained on the basis of ionizations only are plotted as broken lines and the actual t functions as full lines. The simplified and actual curves start at similar values $T(0)$; this is because the dose-weighted energy average of the energy transfers [see Eq. (11)] happens to be close to the W values.

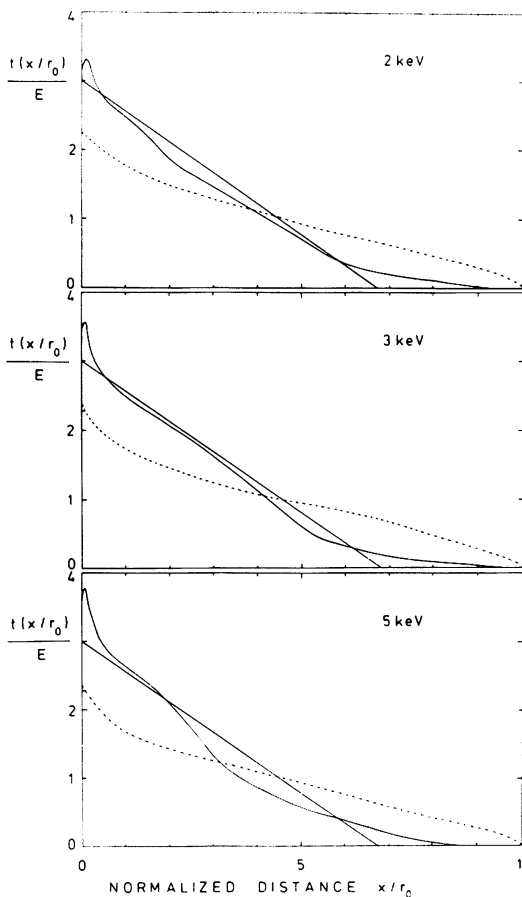


FIG. 10. Comparison of actual proximity functions (solid curves) for electrons with functions that result from simplified models. The broken curves result if the electron tracks are treated as straight line segments with continuous energy loss according to their LET. The solid straight lines result if the tracks are pictured as straight line segments with constant energy loss rate and range equal to two-thirds of the continuous-slowng-down range. Ranges and LET values for water have been used (36).

The results indicate that an experimental method based on ion detection should lead to adequate distance distributions for electrons, and it is not unlikely that this statement should also apply to other charged particles.

CONCLUSION

The present results are a limited contribution toward a systematic collection of distance distributions for different types of radiation. It will be important to extend the calculations to higher energies of electrons, to other particles, and to mixed fields. It will be equally important to compare the results of different Monte Carlo calculations and to determine how sensitive the t functions or other microdosimetric quantities are to inaccuracies of the cross sections that are utilized for the simulated charged particle tracks.

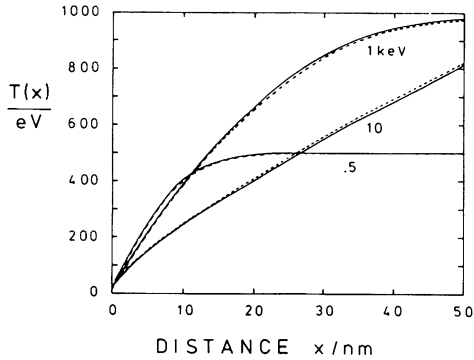


FIG. 11. Integral proximity functions for electrons (solid lines) compared with results of a simplified calculation that utilizes only ionizations (broken lines).

Systematic errors due to faulty cross sections are probably the main source of uncertainty in the results. However, most of the conclusions that one draws from comparing *t* functions at different electron energies should retain their validity, regardless of the fact that details of electron transport may be incorrect.

APPENDIX A

In the following, some essential characteristics of the input data, i.e., the simulated electron tracks, will be given. The program used for the generation of the particle tracks has been described earlier (12). In the simulation an electron is followed until its energy reaches the atomic ionization potential. Elastic scattering, ionization, excitation, reorganization following inner-shell ionization, and similar processes are simulated individually by sampling with representative experimental and theoretical cross sections. The entire trajectories of primary electrons and of all secondaries set in motion are reproduced.

The various cross sections used in the Monte Carlo code are briefly listed in the following. For elastic scattering differential and total Dirac–Mott cross sections have been calculated. For inner-shell ionization (*K* shell of oxygen) Gryzinski (32) cross sections are used. For total excitation and ionization cross sections of various outer shells the Kutcher and Green model (33) is applied. These authors surveyed a wide range of experimental and theoretical investigations and sought to construct a model applicable at all energy levels; this sometimes leads to slight discrepancies with other authors, but the model is convenient and fits a wide energy range. For sampling the energy loss in an inelastic interaction Kim (34, 35), who recommends the use of known values of the oscillator strength for low energy transfers and Mott inelastic cross sections for higher transfers, is followed.

No attempt will be made to give a detailed description of the tracks. However, the limited information that is listed in the following will permit an assessment of essential properties and a comparison with similar data generated by other computer programs.

In Fig. 12 three different ranges (r_i , r_p , and r_s) are plotted versus electron energy; the bands indicate the standard error intervals. The upper band represents the

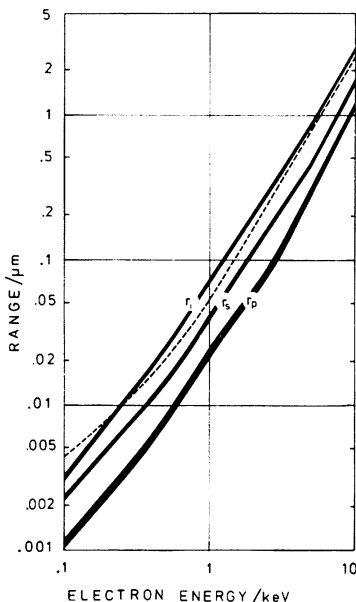


FIG. 12. Integrated range r_i , straight range r_s , and mean projected range r_p for the electron tracks used in the present computations. The width of the bands represents the region of the standard error due to the finite number of tracks that have been utilized. The broken line represents the continuous-slowing-down range r_0 as given by ICRU (36).

mean *integrated* path length r_i of the primary particle from energy E to energy zero. The broken line gives comparison data from ICRU (36) for the continuous-slowing-down range r_0 that is closely related to r_i .

The intermediate band represents what may be termed the mean *straight* range; it is obtained as the mean distance between the starting point at energy E to the last transfer point of the electron.

The lowest band gives what may be termed the mean *projected* range. This is obtained as the mean of the z coordinate of the terminal transfer point, if the electron starts with energy E at $z = 0$ and in the direction of the z axis.

Figure 13 gives, as additional information, the sum distributions of the three different ranges for selected energies. The ordinate value is equal to the fraction p of the 100 tracks that have ranges in excess of the specified value. To keep the graphs simple the standard errors are not indicated. However, they are readily obtained from the formula that applies to the binomial distribution, $p \pm 0.1 \cdot (p \cdot (1 - p))^{1/2}$. For example, one obtains at the 50% level the standard error interval 0.5 ± 0.05 .

In Fig. 14 *isotropic point source kernels* are given for the tracks that have been utilized. They are plotted as shaded bands representing standard error intervals of the fraction of energy that is transferred beyond the specified distance from the starting point of the particle. To facilitate comparison between the curves the distances are given on a logarithmic scale. The solid lines in the upper panel represent point source kernels calculated by Berger (37).

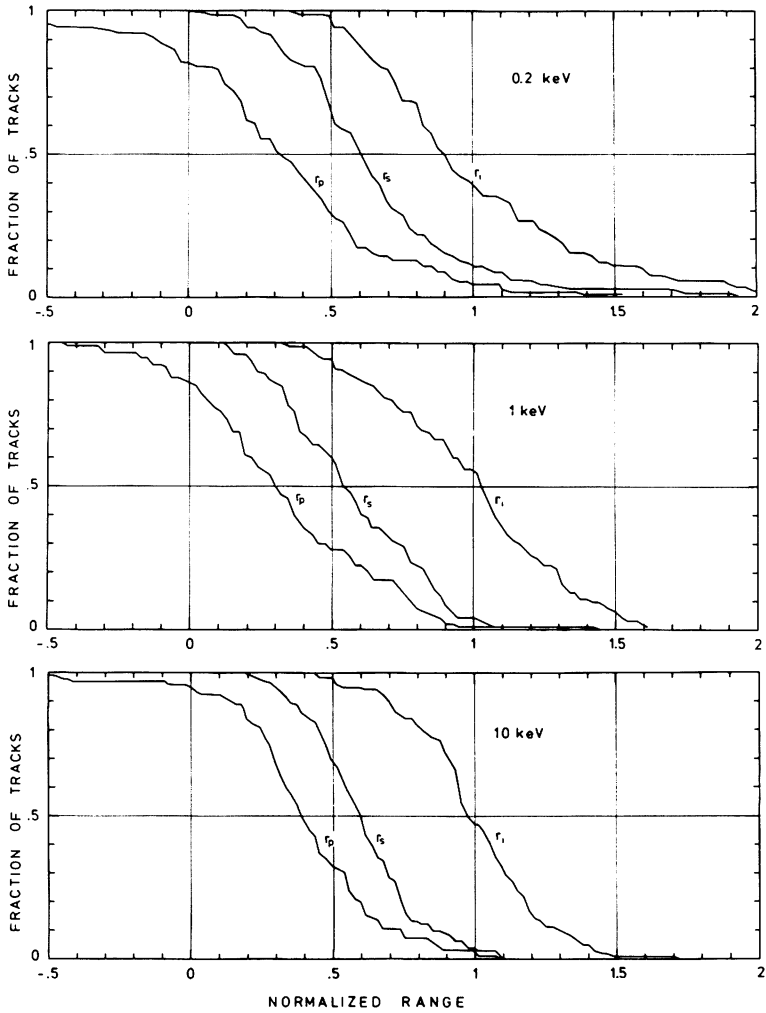


FIG. 13. Sum distributions of the three different ranges of electrons for selected energies. The ordinate value is equal to the fraction of the 100 tracks that have ranges in excess of the specified value. The abscissa value is the range divided by the mean integrated range r_i . Standard errors are not inserted but are readily obtained from the formula given in the text.

It is difficult to judge the degree of error that is due to imprecisions of the cross sections. However, Fig. 15 gives the standard errors of the functions $T(x)$ that are due to the finite number of tracks used in the computation. To avoid intersecting curves such as in Figs. 4 and 5 the function $T_E(x)$ is plotted versus electron energy E and x is used as a parameter. The bands represent the computed values $T_E(x) \pm$ standard deviations. These standard deviations are obtained from the 100 individual values obtained from the 100 particle tracks; the standard deviations never exceed 5%. Figure 15 also has direct biophysical meaning, since the individual curves peak at those electron energies for which the energy concentrations over the specified distances x are largest.

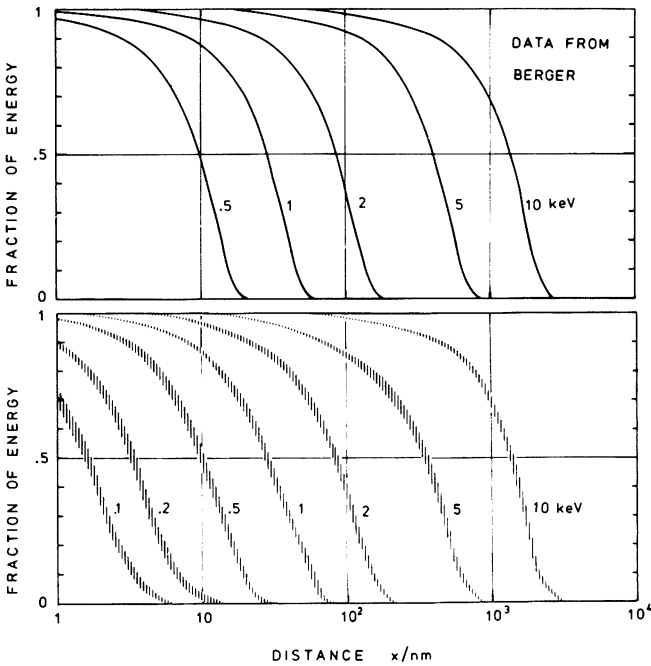


FIG. 14. Normalized isotropic point source kernels for electrons of specified energy. The ordinate is equal to the fraction of energy that is transferred beyond the specified distance from the starting point of the electron. The lower panel gives the results for the simulated tracks used in the present calculations together with their standard deviations. The upper panel gives the kernels derived by Berger (37).

APPENDIX B: INFLUENCE OF DIFFUSION ON THE PROXIMITY FUNCTION

For a diffusion process one may assume that the displacement of a point in a specified direction is normally distributed with mean zero and standard deviation σ . Displacements in orthogonal directions are independently distributed.

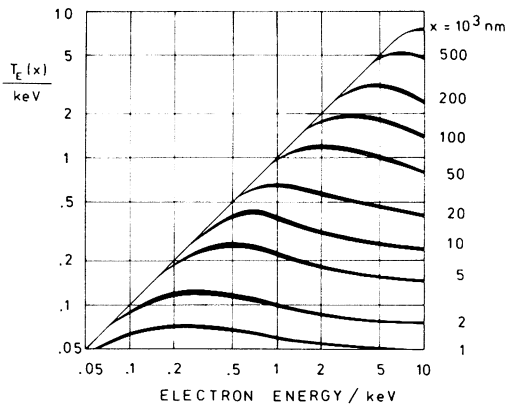


FIG. 15. The integral proximity functions $T_E(x)$ as a function of the initial electron energy E . Different values of the distance x are taken for parameters and are listed at the right ordinate. The bands represent $T_E(x) \pm SD$ obtained from the results for 100 particle tracks.

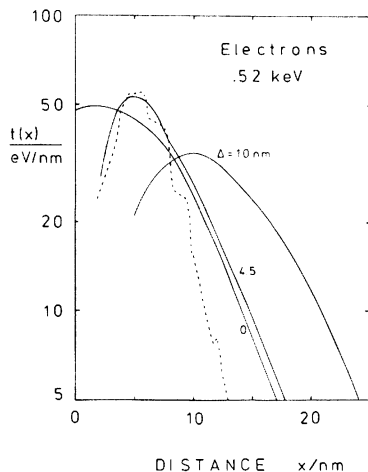


FIG. 16. Comparison of computed proximity functions (solid lines) for 520-eV electrons with proximity function derived from cloud chamber observations (27, 28) (broken line). Two of the computed proximity functions are modified for diffusion with the specified diffusion parameters. Best agreement is obtained with $\Delta = 4.5$ nm.

The parameter σ characterizes the extent of the diffusion; a more meaningful parameter, however, is the average separation Δ that results between two points initially coincident. One finds the following relation between Δ and σ :²

$$\Delta = 4/\pi^{1/2}\sigma \approx 2.26\sigma.$$

Furthermore, one can derive the formula for the proximity function $\bar{i}(x)$ that contains the influence of diffusion:²

$$\bar{i}(x) = \int_0^\infty \frac{x}{2\pi^{1/2}\sigma u} (e^{-(u-x)^2/4\sigma^2} - e^{-(u+x)^2/4\sigma^2})t(u)du.$$

This formula has been applied to obtain the functions in Figs. 6 and 7. In this application the initial δ function has been included in $t(u)$. This implies that the individual transfers are subject to diffusion in themselves; i.e., they do not retain their identity as discrete transfers. This may not always be the situation of interest. For example, cloud chamber observations are based on the observation of droplets that diffuse but that retain their identities as discrete droplets. In this case one will exclude the delta function from the transformation [$\bar{T}(0) = T(0)$].

Figures 16 and 17 give a comparison of proximity functions for electrons of 520 and 955 eV from cloud chamber observations (27, 28) with our results. Best agreement, at least for small distances, is obtained for a diffusion parameter $\Delta = 4.5$ nm; the authors have derived diffusion distances of similar magnitude. There is at present no definite explanation for the fast decline of the observed curves at larger distances x . Certain differences may arise because the computed functions relate to liquid water and the experimental results to gas. However, this cannot account for the marked differences at larger distances.

² A. M. Kellerer, D. Chmelevsky, and H. H. Rossi, in preparation.

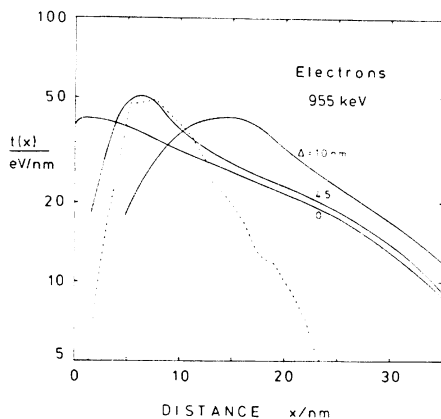


FIG. 17. Comparison of computed proximity functions (solid lines) for 955-eV electrons with proximity function derived from cloud chamber observations (27, 28) (broken line). Two of the computed proximity functions are modified for diffusion with the specified diffusion parameters. Best agreement is obtained with $\Delta = 4.5$ nm.

ACKNOWLEDGMENTS

The authors are indebted to their colleagues Dr. F. Zilker and H. Friede for their extensive contribution to the computational work.

RECEIVED: January 2, 1980; REVISED: May 21, 1980

REFERENCES

1. O. HUG and A. M. KELLERER, *Stochastik der Strahlenwirkung*. Springer-Verlag, Berlin/Heidelberg/New York, 1966.
2. R. S. CASWELL, Deposition of energy by neutrons in spherical cavities. *Radiat. Res.* **27**, 92–107 (1966).
3. R. S. CASWELL and J. J. COYNE, Secondary particle spectra produced by neutron interactions with tissue. In *Proceedings of the First Symposium on Neutron Dosimetry in Biology and Medicine* (G. Burger, H. Schraube, and H. G. Ebert, Eds.), pp. 25–41. Commission of the European Communities, Luxembourg, 1972. [EUR 4896 d-e-f.]
4. M. J. BERGER, Spectrum of energy deposited by electrons in spherical regions. In *Proceedings of the Second Symposium on Microdosimetry, Stresa* (H. G. Ebert, Ed.), pp. 541–559. Commission of the European Communities, Brussels, 1970. [EUR 4452 d-e-f.]
5. M. J. BERGER, Energy deposition by low-energy electrons: Delta-ray effects in track structure. In *Proceedings of the Third Symposium on Microdosimetry* (H. G. Ebert, Ed.), Vol. I, pp. 157–174. Commission of the European Communities, Luxembourg, 1972. [EUR 4810 d-e-f.]
6. U. OLDENBURG and J. BOOZ, Calculation and measurement of neutron produced single-event spectra. *Radiat. Res.* **51**, 551–568 (1972).
7. M. J. BERGER, Some new transport calculations of the deposition of energy in biological materials by low-energy electrons. In *Proceedings of the Fourth Symposium on Microdosimetry, Verbania-Pallanza* (J. Booz, H. G. Ebert, R. Eickel, and W. Walker, Eds.), Vol. II, pp. 695–711. Commission of the European Communities, Luxembourg, 1974. [EUR 5211 d-e-f.]
8. H. G. PARETZKE, Comparison of track structure calculations with experimental results. In *Proceedings of the Fourth Symposium on Microdosimetry, Verbania-Pallanza* (J. Booz, H. G. Ebert, R. Eickel, and W. Walker, Eds.), Vol. I, pp. 141–165. Commission of the European Communities, Luxembourg, 1974. [EUR 5122 d-e-f.]

9. H. G. PARETZKE, G. LEUTHOLD, G. BURGER, and W. JACOBI, Approaches to physical track structure calculations. In *Proceedings of the Fourth Symposium on Microdosimetry, Verbania-Pallanza* (J. Booz, H. G. Ebert, R. Eickel, and W. Walker, Eds.), Vol. I, pp. 123–138. Commission of the European Communities, Luxembourg, 1974. [EUR 5122 d-e-f.]
10. J. P. PATAU, M. MALBERT, M. TERRISSOL, and L. COMMANAY, Etudes dosimétriques dans des cavités sphériques situées en un milieu semi-infini, irradié par des électrons de 2 MeV. In *Proceedings of the Fourth Symposium on Microdosimetry, Verbania-Pallanza* (J. Booz, H. G. Ebert, R. Eickel, and W. Walker, Eds.), Vol. II, pp. 755–778. Commission of the European Communities, Luxembourg, 1974. [EUR 5122 d-e-f.]
11. M. TERRISSOL, J. FOURMENTY, and J. P. PATAU, Détermination théorique des fonctions microdosimétriques pour des électrons de basse énergie dans les gaz. In *Proceedings, Fifth Symposium on Microdosimetry, Verbania-Pallanza* (J. Booz, H. G. Ebert, and B. G. R. Smith, Eds.), Vol. I, pp. 393–406. Commission of the European Communities, Luxembourg, 1976. [EUR 5452 d-e-f.]
12. M. TERRISSOL, *Méthode de simulation du transport d'électrons d'énergie comprise entre 10 eV 30 keV*. Doctorat ès-Sciences No. 839, Université Paul Sabatier, Toulouse, 1978. [Available upon request from the author.]
13. R. N. HAMM, H. A. WRIGHT, J. E. TURNER, and R. H. RICHIE, Spatial correlation of energy deposition events in irradiated liquid water. In *Proceedings, Sixth Symposium on Microdosimetry, Brussels* (J. Booz and H. G. Ebert, Eds.), Vol. I, pp. 179–186. Commission of the European Communities, Harwood, London, 1978. [EUR 6064 d-e-f.]
14. W. E. WILSON and H. G. PARETZKE, Calculation of ionization frequency distributions in small sites. *Radiat. Res.* **81**, 326–335 (1980).
15. D. CHMELEVSKY, *Distributions et moyennes des grandeurs microdosimétriques à l'échelle du nanomètre*. Report CEA-R-4785, 1976. [Available from Service Central de Documentation du C.E.A., C.E.N.-Saclay, B.P. No. 2, 91-Gif-sur-Yvette, France.]
16. D. CHMELEVSKY and A. M. KELLERER, Computation of microdosimetric distributions for small sites. *Radiat. Environ. Biophys.* **14**, 123–136 (1977).
17. A. M. KELLERER and D. CHMELEVSKY, Concepts of microdosimetry. I. Quantities. *Radiat. Environ. Biophys.* **12**, 61–69 (1975).
18. A. M. KELLERER and D. CHMELEVSKY, Concepts of microdosimetry. II. Probability distributions of the microdosimetric variables. *Radiat. Environ. Biophys.* **12**, 205–216 (1975).
19. A. M. KELLERER and D. CHMELEVSKY, Concepts of microdosimetry. III. Mean values of the microdosimetric distributions. *Radiat. Environ. Biophys.* **12**, 321–335 (1975).
20. A. M. KELLERER and W. BELL, Theory of microdosimetry. In *Annual Report on Research Project, 1969–1970*, pp. 73–90. Radiological Research Laboratory, Columbia University, New York, 1970. [Available as NYO-2740-7 from National Technical Information Service, Springfield, VA 22161.]
21. J. W. BOAG, Energy transfer from charged particles. In *Advances in Radiation Research*, Vol. I: *Physics and Chemistry*, (J. F. Duplan and J. Chapiro, Eds.), pp. 9–13. Gordon & Breach, London, 1973.
22. A. M. KELLERER and H. H. ROSSI, Summary of quantities and functions employed in microdosimetry. In *Proceedings of the Second Symposium on Microdosimetry, Stresa* (H. G. Ebert, Ed.), pp. 843–853. Commission of the European Communities, Brussels, 1970. [EUR 4452 d-e-f.]
23. A. M. KELLERER and H. H. ROSSI, A generalized formulation of dual radiation action. *Radiat. Res.* **75**, 471–488 (1978).
24. A. M. KELLERER, Y.-M. P. LAM, and H. H. ROSSI, Biophysical studies with spatially correlated ions. 4. Analysis of cell survival data for diatomic deuterium. *Radiat. Res.* **83**, 511–528 (1980).
25. D. CHMELEVSKY, A. M. KELLERER, and H. H. ROSSI, Concepts of quantities relevant to the evaluation of charged particle tracks. In *Proceedings, Sixth Symposium on Microdosimetry, Brussels* (J. Booz and H. G. Ebert, Eds.), Vol. II, pp. 855–868. Commission of the European Communities, Harwood, London, 1978. [EUR 6064 d-e-f.]
26. H. G. PARETZKE, An appraisal of the relative importance for radiobiology of effects of slow

- electrons. In *Proceedings, Fifth Symposium on Microdosimetry, Verbania-Pallanza* (J. Booz, H. G. Ebert, and B. G. R. Smith, Eds.), Vol. I, pp. 41–48. Commission of the European Communities, Luxembourg, 1976. [EUR 5452 d-e-f.]
27. T. BUDD and M. MARSHALL, Low pressure cloud chamber studies. I. Method of analysis of ionisation distributions. In *Proceedings, Sixth Symposium on Microdosimetry, Brussels* (J. Booz and H. G. Ebert, Eds.), Vol. I, pp. 187–196. Commission of the European Communities, Harwood, London, 1978. [EUR 6064 d-e-f.]
 28. T. BUDD and M. MARSHALL, *Analysis of Ionization Distributions in a Low Pressure Cloud Chamber*. Report AERE-9222, Atomic Energy Research Establishment, Harwell, Oxfordshire, England, 1978.
 29. D. E. CHARLTON and D. V. CORMACK, Energy dissipation in finite cavities. *Radiat. Res.* **17**, 34–49 (1962).
 30. T. E. BURLIN and R. SIMMONS, The dosimetry of radioisotopes incorporated in bone using cavity ionization theory. *Phys. Med. Biol.* **21**, 1–15 (1976).
 31. H. H. ROSSI, Microscopic energy distribution in irradiated matter. In *Radiation Dosimetry, Vol. I, Fundamentals* (F. H. Attix and W. C. Roesch, Eds.), pp. 43–92. Academic Press, New York, 1968.
 32. M. GRYZINSKI, Classical theory of atomic collisions. I. Theory of inelastic collisions. *Phys. Rev.* **138**, 336–358 (1965).
 33. G. J. KUTCHER and A. E. S. GREEN, A model for energy deposition in liquid water. *Radiat. Res.* **67**, 408–425 (1975).
 34. Y.-K. KIM, Energy distribution of secondary electrons. I. Consistency of experimental data. *Radiat. Res.* **61**, 21–35 (1975).
 35. Y.-K. KIM, Energy distribution of secondary electrons. II. Normalization and extrapolation of experimental data. *Radiat. Res.* **64**, 205–216 (1975).
 36. ICRU, *Linear Energy Transfer*. Report. No. 16, International Commission of Radiation Units and Measurements, Washington, DC, 1970.
 37. M. J. BERGER, *Improved Point Kernels for Electron and Beta-Ray-Dosimetry*. Report NBSIR 73-107, National Bureau of Standards, Washington, DC, 1973.